2019-06

CONSTRUCTION, OPERATION, AND DESIGN IMPROVEMENT OF A SMALL-SCALE LIQUID AIR ENERGY STORAGE SYSTEM PROTOTYPE

Amalla, Sammy

Monterey, CA; Naval Postgraduate School

NAVAL POSTGRADUATE SCHOOL

MONTEREY, CALIFORNIA

THESIS

CONSTRUCTION, OPERATION, AND DESIGN IMPROVEMENT OF A SMALL-SCALE LIQUID AIR ENERGY STORAGE SYSTEM PROTOTYPE

by

Sammy Amalla

June 2019

Thesis Advisor:	Anthony G. Pollman
Co-Advisor:	Alejandro S. Hernandez
Second Reader:	Gary W. Parker

THIS PAGE INTENTIONALLY LEFT BLANK

REPORT DOCUMENTATION PAGE	*Form Approved OMB No. 0704-0188*

1. AGENCY USE ONLY *(Leave blank)*	**2. REPORT DATE** June 2019	**3. REPORT TYPE AND DATES COVERED** Master's thesis

4. TITLE AND SUBTITLE
CONSTRUCTION, OPERATION, AND DESIGN IMPROVEMENT OF A SMALL-SCALE LIQUID AIR ENERGY STORAGE SYSTEM PROTOTYPE

5. FUNDING NUMBERS

6. AUTHOR(S) Sammy Amalla

7. PERFORMING ORGANIZATION NAME(S) AND ADDRESS(ES)
Naval Postgraduate School
Monterey, CA 93943-5000

8. PERFORMING ORGANIZATION REPORT NUMBER

9. SPONSORING / MONITORING AGENCY NAME(S) AND ADDRESS(ES)
Office of Naval Research

10. SPONSORING / MONITORING AGENCY REPORT NUMBER

11. SUPPLEMENTARY NOTES The views expressed in this thesis are those of the author and do not reflect the official policy or position of the Department of Defense or the U.S. Government.

12a. DISTRIBUTION / AVAILABILITY STATEMENT
Approved for public release. Distribution is unlimited.

12b. DISTRIBUTION CODE
A

13. ABSTRACT (maximum 200 words)

Islanded renewable power sources require energy storage to mitigate intermittency. Liquid air energy storage (LAES) systems provide a novel alternative to the usual battery bank or fossil-fueled backup generator. LAES systems combine and leverage three mature technologies: cryogenics, expansion turbines, and induction generation. Although LAES has a lower round trip efficiency, the capital and maintenance costs are much lower than battery storage. LAES system performance is comparable to both pumped hydro storage (PHS) systems and compressed air energy storage (CAES) systems, but with the advantage of harnessing low-entropy waste heat or cold from co-located processes. An LAES system footprint is also a fraction of the size of a CAES or PHS system with a similar storage capacity. This study employed experiments to support a model-based systems engineering approach. A LAES system prototype was built from mature off-the-shelf components and utilized surplus, renewable, micro grid power in an attempt to liquefy ambient air via the Joule-Thompson effect. Collected performance data was compared to specifications provided with a previously failed system to identify and correct shortfalls for this system. Two potential design improvements were examined, and a benefit analysis was presented to inform future construction and testing necessary to inform the modeling and simulation of a building-scale LAES system and support the production of a fully functional prototype.

14. SUBJECT TERMS
energy storage, Linde-Hampson Cycle, liquid air energy storage, compressed air energy storage, renewable energy, cryogenics, model-based systems engineering (MBSE)

15. NUMBER OF PAGES
59

16. PRICE CODE

17. SECURITY CLASSIFICATION OF REPORT	**18. SECURITY CLASSIFICATION OF THIS PAGE**	**19. SECURITY CLASSIFICATION OF ABSTRACT**	**20. LIMITATION OF ABSTRACT**
Unclassified	Unclassified	Unclassified	UU

NSN 7540-01-280-5500

Standard Form 298 (Rev. 2-89)
Prescribed by ANSI Std. 239-18

THIS PAGE INTENTIONALLY LEFT BLANK

Approved for public release. Distribution is unlimited.

CONSTRUCTION, OPERATION, AND DESIGN IMPROVEMENT OF A SMALL-SCALE LIQUID AIR ENERGY STORAGE SYSTEM PROTOTYPE

Sammy Amalla
Lieutenant, United States Navy
BSEE, The Citadel, 2013

Submitted in partial fulfillment of the
requirements for the degree of

MASTER OF SCIENCE IN SYSTEMS ENGINEERING

from the

NAVAL POSTGRADUATE SCHOOL
June 2019

Approved by: Anthony G. Pollman
Advisor

Alejandro S. Hernandez
Co-Advisor

Gary W. Parker
Second Reader

Ronald E. Giachetti
Chair, Department of Systems Engineering

THIS PAGE INTENTIONALLY LEFT BLANK

ABSTRACT

Islanded renewable power sources require energy storage to mitigate intermittency. Liquid air energy storage (LAES) systems provide a novel alternative to the usual battery bank or fossil-fueled backup generator. LAES systems combine and leverage three mature technologies: cryogenics, expansion turbines, and induction generation. Although LAES has a lower round trip efficiency, the capital and maintenance costs are much lower than battery storage. LAES system performance is comparable to both pumped hydro storage (PHS) systems and compressed air energy storage (CAES) systems, but with the advantage of harnessing low-entropy waste heat or cold from co-located processes. An LAES system footprint is also a fraction of the size of a CAES or PHS system with a similar storage capacity. This study employed experiments to support a model-based systems engineering approach. An LAES system prototype was built from mature off-the-shelf components and utilized surplus, renewable, micro grid power in an attempt to liquefy ambient air via the Joule-Thompson effect. Collected performance data was compared to specifications provided with a previously failed system to identify and correct shortfalls for this system. Two potential design improvements were examined, and a benefit analysis was presented to inform future construction and testing necessary to inform the modeling and simulation of a building-scale LAES system and support the production of a fully functional prototype.

THIS PAGE INTENTIONALLY LEFT BLANK

TABLE OF CONTENTS

THIS PAGE INTENTIONALLY LEFT BLANK

LIST OF FIGURES

THIS PAGE INTENTIONALLY LEFT BLANK

LIST OF TABLES

THIS PAGE INTENTIONALLY LEFT BLANK

LIST OF ACRONYMS AND ABBREVIATIONS

ASME	American Society of Mechanical Engineers
CAES	compressed air energy storage
DoD	Department of Defense
DoN	Department of the Navy
COTS	commercial-off-the-shelf
E2O	Expeditionary Energy Office
ES2	Energy Security and Sustainability
FOB	forward operating base
JT	Joule-Thompson
LAES	liquid air energy storage
LMTD	log mean temperature difference
MBSE	model based system engineering
MERV	minimum efficiency reporting value
NAVFAC	Naval Facilities Engineering Command
NIST	National Institute of Standards and Technology
NPS	Naval Postgraduate School
OASD	Office of the Assistant Secretary of Defense
ONR	Office of Naval Research
OPNAVINST	Chief of Naval Operations instruction
PHS	pumped-hydroelectric storage
PTFE	polytetrafluoroethylene
RHX	regenerative heat exchanger
SCFM	standard cubic feet per minute
SECNAV	Secretary of the Navy
USN	United States Navy
USMC	Unites States Marine Corps

THIS PAGE INTENTIONALLY LEFT BLANK

EXECUTIVE SUMMARY

As the single largest energy consumer in the world, the Department of Defense (DoD) accounts for approximately 80% of the energy consumed by the U.S. federal government (Hicks 2017). A Pentagon study focused on conflicts in the Middle East found that through 2009, more than 3000 soldiers and contractors were killed or wounded protecting convoys carrying fuel (Douquet 2017). This steady stream of trucks required to fuel a style of war dating back to World War II presents a significant vulnerability to U.S. forces. This vulnerability is the motivation for several energy initiatives throughout the DoD.

In FY2011, as part of the *Annual Energy Management Report* (AEMR), the DoD released its Energy Performance Master Plan. It promoted investments into renewable energies, reduction through efficiency, and increased resilience through future technologies (OASD [EI&E] 2018). The master plan also established metrics to measure progress toward performance goals. The individual services followed suit with implementation of their own policies and individual goals as well. The Department of the Navy set out on an aggressive goal of 50% reduction in facilities energy usage as well as 50% of their shore installation to be net zero energy consumers by 2020 (Navy Office of Information 2012). The Marines are investigating methods to optimize soldier's loads to decrease fuel load requirements through the United States Marine Corps Energy Expeditionary Office (E^2O) (Marine Corps Expeditionary Energy Office 2011). In addition, the Marines view this as an opportunity to become more lethal through increased operational reach (Pollman 2013). The Army's focus on increased efficiency and distributed renewable energy is outlined in their Energy Security and Sustainability (ES^2) Strategy. In FY2016, the Army surveyed 143 installations and over 43 of them were well on their way to meeting the goal of 30% reduction in their usage as compared to a 2003 baseline, by 2020.

To align with the goals of the National Defense Strategy for increased energy security and energy resilience, a significant shift to implement renewable energy technologies like solar and wind is sweeping across the DoD. A major drawback for

quickly adopting renewable energy systems at stateside installations are periods of excess power and system shortages, or intermittency. Intermittency is prevented through the storage of excess power, usually in the form of batteries of diesel generators, and subsequently released during shortage periods to balance the power load. This thesis presents Liquid Air Energy Storage (LAES) systems as a viable alternative solution, completely independent of fossil fuels.

LAES systems utilize excess power from renewable sources to power equipment necessary for the liquefaction of air. The air is stored in liquid form in a vacuum insulated canister at a low pressure. During periods of power shortages, the liquid air is expanded by exposing it to ambient temperatures and forced through a turbine attached to a generator the produces the power necessary to meet demand.

This study investigated a LAES prototype currently in the Naval Postgraduate School's (NPS's) possession that had failed to produce liquid air. The prototype utilized a precooled Linde–Hampson cycle to liquefy air. Due to the large temperature changes required, the main heat exchanger performance is key to successful system operation. It is required to cool incoming air from 277K to 177K or less. Thermodynamic analysis was performed on the current system to identify the root cause of the failure, which was determined to be the size of the regenerative heat exchanger shell tubing. The tubing restricted return airflow by limiting the flow diameter to about half of the design specification. Because of this restriction, the system was only able to provide about two-thirds the required cooling capacity. Operational data from the inherited system, previously unavailable for prior research conducted at NPS, was obtained. Operational parameters, such as system pressures and flows were varied to attempt to overcome the flow restriction due to the smaller RHX shell tubing but were beyond the capacity of the installed equipment. This did demonstrate, however, that higher flows provided improved performance. Further log mean temperature difference based thermal analysis was conducted on the current system design to explore the potential of the system if corrected.

After identifying the cause of failure, analysis was conducted to explore two new heat exchanger designs for the system. The first was a compact spiral tube shell and tube heat exchanger that provided 45ft^2 of heat transfer surface area while only occupying six-

cubic-feet. This would potentially provide at least ten times the cooling capacity needed for liquefaction of air. This performance did come with a cost of $30k and a weight of about 800 pounds. The second design utilized a brazed-fin tube design. The length of the heat exchanger would be reduced from 100 feet to 40 feet, but the heat transfer surface area increased by four times compared to the original design. This design would be similar to the current design with the addition of fins and a larger shell tube size to accommodate them. The finned tube design would still reduce the heat exchanger volume by about 40%. The major drawback is possibility of repeating some of the fabrication issues inherent to the current design. The tubes would require hand bending in a mandrel pipe bender, and connection fittings would have to be installed in-house on each 20-foot section. This could lead to damaging the fins or leaks within the system eliminating the benefit of the redesign. The finned tube design is significantly cheaper than the spiral tube design, at $3.50 per watt, as compared to over $8 per watt, but does come with much more risk. Both designs promote mobility for future iterations, but the stakeholder would have to decide how much risk they are willing to accept for added performance.

This thesis provides the operational data of the current system at NPS that was lacking in previous research. It also provides improved designs for the current system and their potential benefits to assist in producing a working prototype. Future researchers can utilize the operational analysis to examine the trade-space in the modeling and simulation of a building scale system.

References

ASAIE, Department of the Army. 2015. *Energy Security and Sustainability Strategy.*RefID: 2–204FF1C. March 03. https://www.army.mil/e2/c/downloads/394128.pdf.

Douquet, Greg. 2017. “Unleash Us From the Tether of Fuel.” Atlantic Council. January 11, 2017. Accessed May 01, 2019. https://www.atlanticcouncil.org/blogs/defense-industrialist/unleash-us-from-the-tether-of-fuel.

Hicks, Sierra. 2017. “Fact Sheet: Powering the Department of Defense.” American Security Project. September 18, 2017. https://www.americansecurityproject.org/fact-sheet-powering-the-department-of-defense/.

Marine Corps Expeditionary Energy Office. 2011. *Marine Corps Expeditionary Energy Strategy and Implementation Plan*. Washington, DC: Marine Corps Expeditionary Energy Office Headquarters.

Navy Office of Information. January 21, 2010. "USDA, Navy Sign Agreement to Encourage the Development, Use of Renewable Energy." Accessed April 15, 2019. https://www.navy.mil/submit/display.asp?story_id=50710.

Office of the Assistant Secretary of Defense for Energy, Installations and Environment. (2017). *Annual Energy Management and Resilience (AEMR) Report*. 7. https://www.acq.osd.mil/eie/Downloads/IE/FY%202017%20AEMR.pdf

Pollman, A.G. 2013. "Energy Optimization: A Combat Multiplier." *Marine Corps Gazette* 97 (11): 69–73.

T

ACKNOWLEDGMENTS

I would like to thank my loving wife for always pushing me to exceed my own expectations. Thank you for the understanding and support to make these past two years possible. I am grateful that you kept the home front secure while wrangling our adventurous daughter and preparing to bring our son into the world. You are an amazing wife and superhero mother: without your unwavering motivation and drive, this would not have been possible.

I would like to thank Dr. Pollman for providing the occasional vectoring needed to focus my efforts. Your support and confidence throughout the thesis process were much appreciated.

THIS PAGE INTENTIONALLY LEFT BLANK

I. INTRODUCTION

A. MOTIVATION AND BACKGROUND

Despite many U.S. Department of Defense (DoD) energy initiatives, the steady stream of fuel trucks to feed the military's antiquated way of war provides a significant vulnerability to U.S. forces. A Pentagon study focused on conflicts in the Middle East found that through 2009, over 3000 troops and civilian contractors were killed or wounded protecting convoys, 80% of which were carrying fuel (Douquet 2017). To support operations in Afghanistan in 2011, USMC Forward Operating Bases (FOBs) were consuming approximately 200,000 gallons of fuel per day. Transporting this fuel over long distances and dangerous terrain via convoy resulted in the casualty of one soldier per 50 convoys over a three-month period (Pollman 2013). Since 1976, this reliance on fossil fuels has driven the defense of shipping lanes around the world at a cost of about $8 trillion for the DoD to maintain at least one aircraft carrier in the Persian Gulf charged with protecting oil cargoes in the area (Hicks 2017).

The DoD is the largest single consumer of energy in the world, accounting for almost 80% of the total energy consumed by the federal government (Hicks 2017). To ensure mission readiness the DoD has made the pursuit of energy security and resilience its chief priority (OASD (EI&E) 2017). The 2018 National Defense Strategy outlines a security environment characterized by near peer competition in a disruptive battlefield and conducted at higher speeds and longer distances, where U.S. citizens are not safe within their own borders (OASD n.d.). The ability to leverage the capabilities of weapons platforms, facilities, and equipment through energy resilience, requires it to be included in strategic discussions as a force multiplier (OASD [EI&E] 2017).

In FY2011, the Energy Performance Master Plan was developed and released with that year's Annual Energy Management Report. It outlined the framework for decision-making across all departments and outlined metrics for evaluating progress toward energy goals. The following key elements were included (OASD [EI&E] 2017, C-1):

1. Increase supply through renewable energies,

2. Reduce demand by maximizing efficiency,

3. Enhance energy resilience by adapting future forces and technologies

According to Hicks, "In 2012, the Defense Department made a commitment to install three gigawatts of renewable generating capacity, one from each of the Army, Navy, and Air Force installations by 2025" (2017, 2). The individual branches of service are taking it upon themselves to help reduce this energy burden as well.

In FY2016, the Department of the Navy (DoN) accounted for 28% of the DoD's facilities energy cost. This is after a 22% reduction in energy usage from 2003–2015, with an additional 6.7% reduction between 2015 and 2016. In 2014 through 2018, the Navy each year achieved its yearly goal of producing or procuring 25% or more of its energy though renewable sources. In 2016, the percentage was as high as 28% (OASD[EI&I] 2017). The Navy has even more aggressive goals for the future, to include a 50% reduction of their facilities' energy usage, as well as 50% of their shore installation to be a net zero energy consumer by 2020 (Navy Office of Information 2012).

In testimony to Congress, then Lieutenant General James Mattis stated that the military must be "unleashed from the tether of fuel" (Douquet 2017). The United States Marine Corps Energy Expeditionary Office (E^2O) was established within the DoD as a result of this testimony to investigate soldier load optimization for fuel and power requirements (Marine Corps Expeditionary Energy Office 2011).

The Army followed suit with its Energy Security and Sustainability (ES^2) Strategy, which is focused on increasing efficiency and transitioning to distributed renewable energy sources (United States Army 2015). According to OASD (2017), 9.5% of the U.S. Army's energy use was supplied from renewable sources in FY2016, and the Army is well on its way to meet its commitment to one gigawatt of renewable energy installed by 2025. Of 143 installations surveyed, at least 43 were positioned to meet their goal of 30% energy reduction compared to a FY2003 baseline.

To align with the goals of the National Defense Strategy for increased energy security and energy resilience, DoD is experiencing a significant shift towards

implementing renewable technologies like solar and wind power generation. Due to the inherent intermittency, solar and wind power generation alone are not enough to promote energy resilience. To remain uninterrupted, these systems rely on energy storage systems. In times where electrical generation is greater than demand, the energy storage system uses the excess power to store energy for release during shortage periods to balance electrical loading (Wang et al. 2015).

B. LIQUID AIR ENERGY STORAGE

A major drawback to quickly adopting renewable energy systems stateside at installations are periods of excess power and system shortages, or intermittency. When electrical generation is higher than the demand, energy storage systems use the excess power to store energy and then release power during shortages in order to balance electrical loads (Wang et al. 2015). Many methods are available to provide the energy storage necessary to overcome this intermittency, to include rechargeable batteries, compressed air, pumped hydro, and liquid air. The current method of using diesel generators is counter to the DoD's energy goals of reducing dependency on fossil fuels. Batteries provide a simple solution, but can be costly overtime due to maintenance and replacement expenses. They also utilize rare metals further exposing another vulnerability through possible supply chain interruptions. Traditional compressed air energy storage (CAES) systems require large undergrounds caverns for use as storage vessels (McLarnon and Cairns 1989). Pumped hydro requires two large co-located and connected bodies of water to facilitate storage. These geographic constraints prevent CAES and pumped hydro from being viable options for remote locations and forward operating bases (FOBs). Micro-CAES eliminate the geographic constraint of the traditional system through the use of smaller pressurized vessels. This approach is inferior to liquid air, due to reduced energy density per unit volume (Ameel et al. 2013, Kim et al. 2012). Although still considered a developing technology, liquid air employs methods used since the early 1960s in the natural gas industry (Castillo and Dorao 2013). Excess energy from renewable sources, such as wind and solar, provide the required power for the cryogenic cycle used in the liquefaction of air to be stored for later use. The liquefied air is exposed to ambient temperatures, where it

expands to 700 times its liquid volume, and directed through an expansion turbine attached to a generator to produce the supplemental power necessary to balance the power load.

The simplest method to liquefy air is the Linde-Hampson cycle, which requires a compressor, a two-flow heat exchanger, and a Joule Thompson (JT) valve (Hands 1986). Other methods include Claude cycle, Linde cycle, precooled Linde-Hampson cycle, and other variations (Barron 1985). The precooled Linde-Hampson cycle is the method used in this research, and its application will be described in detail in the next chapter.

C. THESIS OVERVIEW

The preceding sections provide the motivation, background, and an introduction to the LAES system. Chapter II presents the component identification during system reconstruction and basic operational overview of the current LAES system in possession at the Naval Postgraduate School (NPS). Chapter III provides the results of the system baselining operations and subsequent thermodynamic analysis of the results. Chapter IV proposes potential system design improvements and provides a theoretical analysis of their effects on system performance.

This thesis applies a model-based systems engineering (MBSE) approach to constructing a building scale LAES system. It focuses on the construction and operation of a small-scale prototype. Once it is operational, it will provide performance data to be validated against a software prototype model previously developed by Willis (forthcoming). Using MBSE eliminates the need to perform physical tests on multiple prototypes in this phase of design, while exploring the system trade space. Figure 1 illustrates the systems engineering V-model and where the work included in this thesis falls within the system design process.

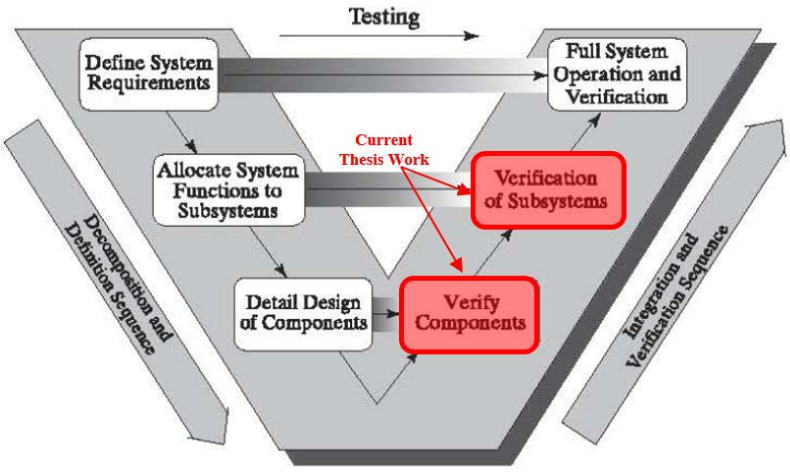

Figure 1. V-Model Identifying Application of Thesis Work. Adapted from Blanchard and Fabrycky (2010).

This thesis utilized the operational principles for the LAES system developed through previous work completed by Howe in 2018 as the basis for system operation and testing. Howe (2018) developed an expected yield of liquid nitrogen through a closed-form thermodynamic analysis of the Linde–Hampson cycle. The steps following this thesis include modeling and simulation of a building scale LAES system to meet a specified demand, as well as the implementation of new designs discussed in this thesis. Chapter V closes out this thesis and provides a description of future work.

THIS PAGE INTENTIONALLY LEFT BLANK

II. MATERIAL AND METHODS

A. COMPONENT IDENTIFICATION

In 2015, the Office of Naval Research (ONR) sponsored the building of a demonstration Liquid Air Energy Storage (LAES) System. Naval Facilities Engineering Command (NAVFAC) Engineering and Expeditionary Warfare Command took on the project, and contracted Nitro-Turbodyne Inc. to build the system. The system was not successful in producing liquid air. The Naval Postgraduate School (NPS) now has possession of the system to continue research into the feasibility of constructing a building scale LAES system. Figure 2 provides a schematic of the LAES system designed by Nitro-Turbodyne. The system consists of two major sections: the liquefaction portion outlined in blue, and the expansion portion outlined in red.

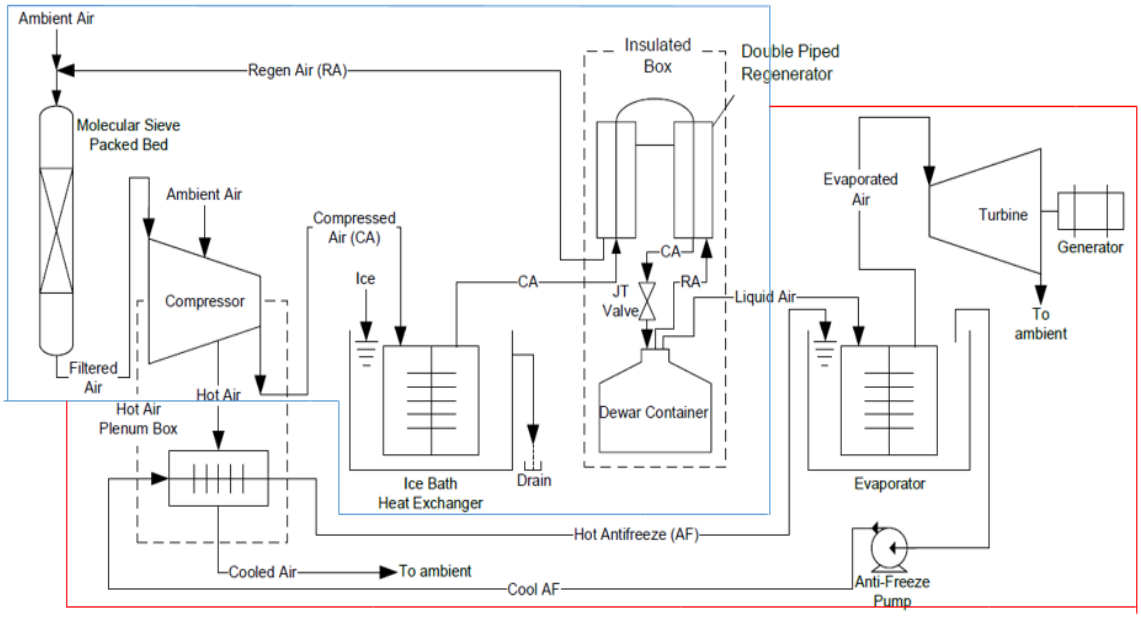

Figure 2. Nitro-Turbodyne LAES System Schematic. Adapted from Nitro-Turbodyne (2016a).

Due to the disassembly of the system for shipment and the lack of operational data from initial testing, baselining the system was a necessity. Initial efforts focused on

component identification and subsequent reassembly. The liquefaction subsystem consists of a molecular sieve, a compressor, an ice water heat exchanger, a double-piped counter-current regenerative heat exchanger (RHX), a JT valve, and a dewar. The molecular sieve shown in Figure 3 removes moisture and CO_2 from ambient air by using a mixed bed of sorbent 4A and sorbent 13X (Nitro-Turbodyne 2016a).

Figure 3. Mixed Bed Molecular Sieve

The removal of water and CO_2 from the system eliminates the concern for the fluids freezing prior to the production of liquid air, since water freezes at 273.15K and CO_2 freezes at 194.75K (Lemmon, McLinden, and Friend 2008). What remains is 78.12% nitrogen, 20.96% oxygen, and 0.92% Argon (Lemmon, Jacobsen, Penoncello, and Friend 2000). The sieve housing consists of a 6-foot-long 4-inch diameter section of PVC piping with wire mesh on either end to hold the approximately 25 pounds of sorbent material in place. The intake side of the sieve includes a 13 minimum efficiency reporting value (MERV) filter material to prevent the intake of particulate material larger than 3.0 microns that could potentially damage the compressor. The compressor shown in Figure 4 is a commercial oil-free breathing-air compressor manufactured by AireTex capable of providing 3600 psi air at a rate of 4.6 standard cubic feet per minute (SCFM) (Nitro-Turbodyne 2016b).

Figure 4. AireTex 45 Oil-Free Air Compressor as Part of the Nitro-Turbodyne LAES System. Source: Nitro-Turbodyne (2016b).

The ice-water heat exchanger shown in Figure 5 consists of a 20-foot-long coiled section of quarter-inch outside-diameter stainless steel tubing fitted with 2.25 in^2 aluminum fins, spaced about one-inch apart along the length of the coil.

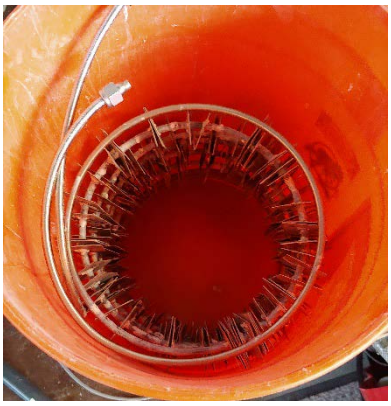

Figure 5. Ice-Water Heat Exchanger

The heat exchanger coil is submerged in a plastic five-gallon bucket filled with enough ice and water to fully cover the coil assembly. The purpose of the ice-water heat exchanger is to reduce temperature of the air exiting the compressor to near 0˚C. The regenerative heat exchanger shown in Figure 6 is a counter-current double-tubed heat exchanger used to precool the incoming air prior to it reaching the JT valve.

Figure 6. Regenerative Heat Exchanger

The primary, or tube side of the heat exchanger, consists of 100 feet of 0.25-inch outside diameter 304 stainless steel tubing wrapped with 0.125-inch thick round copper wire to promote turbulent flow. The secondary, or shell side of the heat exchanger, consists of 80-feet of polytetrafluoroethylene (PTFE) corrugated tubing and 20-feet of polyethylene corrugated tubing. Detailed inspection revealed the outside diameter of the secondary was actually only 0.75-inches vice the supplied specification of 1-inch. Wrapping polypropylene tube insulation around the outside of the secondary side of the RHX minimizes heat losses to the external environment. The valve previously used as the JT valve was not readily apparent, which is a pressure-reducing device that maintains a constant enthalpy of the air as it passes through it. Installation of a stainless steel bodied needle valve, shown in Figure 7, with a PTFE seat was necessary to accomplish this task. It was fitted with a remote operating handle. The final component of the liquefaction system is the dewar, also shown in Figure 7, which is a 25-liter vacuum-insulated container manufactured by Taylor Wharton to store the cryogenic fluid at 79K.

Figure 7. 25-Liter Dewar with JT Valve

The RHX, JT valve, and dewar were previously placed inside of a large plywood box (regenerative tower) filled with fiberglass matte insulation that was open on the bottom two feet, exposing the dewar and the underside of the RHX coil to ambient temperatures. The regenerative tower assembly was replaced with a 72-inch tall concrete form tube with a 24-inch diameter. It was filled with about 75-pounds of Green Fiber blown insulation to fully insulate the RHX, JT valve, and dewar.

B. OPERATION OVERVIEW

Figure 8 is a block diagram of the liquefaction process from the Nitro-Turbodyne LAES system to aid in following the operational process within the system.

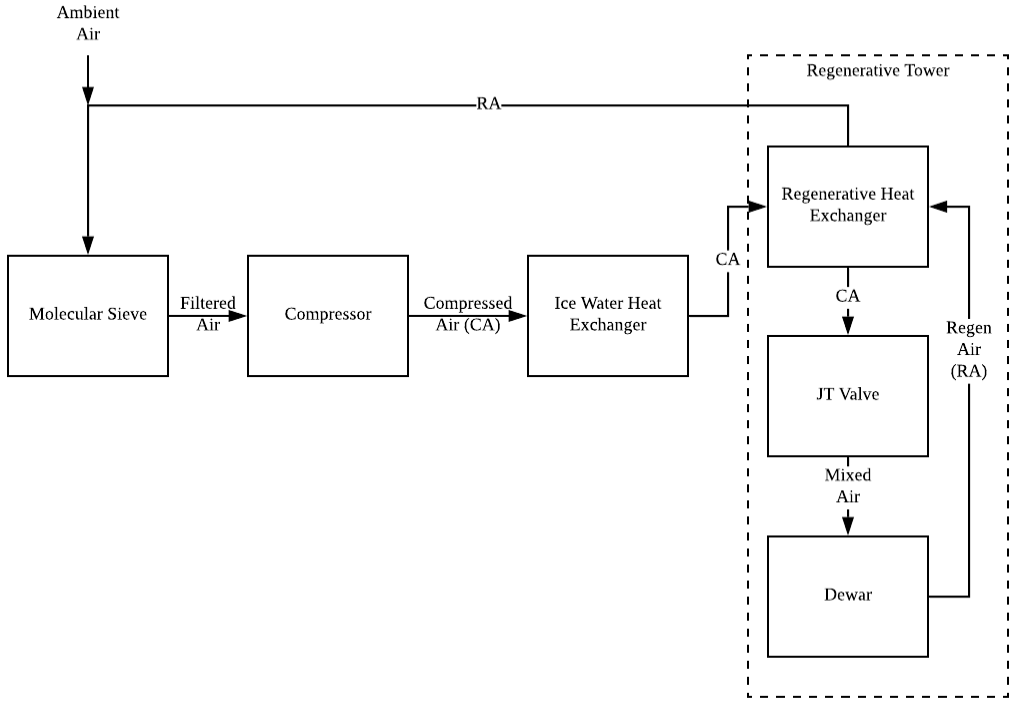

Figure 8. Block Diagram of Nitro-Turbodyne LAES system Liquefaction Process

The LAES system takes ambient air into the molecular sieve, and removes any moisture, particulate, and carbon dioxide from the incoming air. The now-filtered air enters the compressor, where it is compressed from ambient pressure to about 3500 psi via a sequential three-stage process. As the pressure increases, the temperature increases as well. The fins on the casing of each stage and the attached fan cool the air between stages by convection. According to AireTex, the exiting air is within 10˚C of ambient temperature. The warm high-pressure air passes into the ice-water heat exchanger to cool it to near 0˚C prior to its entry into the double-tubed RHX. The RHX transfers the compressed air to the inlet side of the JT valve. The JT valve reduces the pressure of the compressed air from about 250 atmospheres to near ambient pressure. Due to the significant pressure drop experienced during this expansion, the temperature decreases considerably as well. If the temperature of the compressed air delivered to the JT valve is low enough, the discharge of the JT valve will be a mixture of liquid and gaseous air. Air is required to be at or below

78.9K to become a liquid (Lemmon, Jacobsen, Penoncello, and Friend 2000). As air passes through the JT valve it undergoes a throttling process, a process in which pressure drops and temperature either drops or increases, while enthalpy remains unchanged (Moran and Shapiro 2004, 549–550). The required JT valve inlet temperature can be determined by referencing enthalpy value at the required 78.9K and atmospheric pressure, and then referencing the same enthalpy at the JT valve inlet pressure to find the corresponding temperature. The demister filter attached to the outlet of the JT valve separates the liquid air from the stream, and allows it to fall to the bottom of the dewar where it is retained for later use. The remaining gaseous, or regenerative, air cycles back into the RHX, where it precools the incoming compressed air on its way to the JT valve. The regenerative air returns to the inlet of the molecular sieve and combines with ambient air to make up for gaseous volume lost in the liquefaction process.

THIS PAGE INTENTIONALLY LEFT BLANK

III. CURRENT SYSTEM

A. SYSTEM BASELINE

According to Nitro-Turbodyne, the system should theoretically be able to go from a "cold start" to producing liquid in approximately 3–4 hours. A cold start means the entire system is depressurized and at or near ambient temperature. To baseline the system, it was initially operated in accordance with Nitro-Turbodyne's provided operating manual. The ice-water heat exchanger required 20 pounds of ice and some additional water for it to provide total coverage of the heat exchanger. The compressor was isolated from the system and started to allow it to build up to an operating pressure of about 3500 psig. Once the pressure stabilized, a controlled pressurization of the rest of the system was conducted, utilizing the compressor discharge valve. Throttling the JT valve to allow 2–5 psig of pressure into the dewar, commenced the cool-down of the incoming air through the RHX. The industrial controller supplied with the system provided continuous monitoring capabilities for compressor discharge pressure, dewar pressure, and dewar temperature. The JT valve position required frequent adjustment to maintain a constant cool-down rate. Operating the system in this manner for approximately six hours, at which time the cool down stalled, achieved a minimum dewar temperature of 239K (-34˚C). The system was operated again, with a higher return flow rate through the RHX. This was achieved by maintaining dewar pressure near 10 psig. This new method was slightly more successful by achieving a minimum temperature of 218K (-51˚C). The final method used in operating the original system required charging the system with liquid nitrogen, facilitating a "hot start." According to Nitro-Turbodyne, the hot start should produce liquid after about 15 minutes of operation. This method lowers the dewar's temperature to 78K (-195˚C), the temperature required for liquefaction of the air through the JT valve. The compressor provided the required suction to pump the liquid nitrogen through an outlet connection reserved for the expansion portion of the future power generation section. Upon reaching the liquefaction temperature, the system's suction was switched from the liquid nitrogen source, to a mixture of ambient air and return air from the RHX. After realignment, system operation was continued for two more hours while, dewar pressure again was maintained

near 10 psig. While in operation, temperature steadily increased until leveling off near 213K (-60˚C). This operational data provided some insight into why the system was previously unsuccessful as well as some possible modification. Table 1 provides a summary of the baseline results obtained.

Table 1. Summary of Baseline Operational Data

Method	Dewar Operating Pressure	Resultant Temperature
Cold Start	2-5 psig	-34 ˚C
Increased Dewar Pressure	10 psig	-51 ˚C
Hot Start	10 psig	-60 ˚C

These results confirmed previously identified shortcomings of the recommended operating parameters. They also illustrate how modifying the dewar operating pressure subsequently affected system performance. The next section will provide an in-depth thermodynamic analysis of the current system's regenerative heat exchanger.

B. ANALYSIS OF THE CURRENT REGENERATIVE HEAT EXCHANGER

To begin the analysis, the system requirements were first be explicitly identified. The requirements in their most basic form were to take in ambient air and process it through a series of compression and expansion cycles, resulting in the cool-down needed to store it at low temperature and pressure. The key contributor to this process in the system is the RHX and is the main focus for this analysis. The amount of heat energy from the incoming air requiring removal was determined to evaluate the effectiveness of the RHX. First, the enthalpy value corresponding to the air liquefaction temperature of 78.9K at atmospheric pressure was identified, and then the same enthalpy value at the JT valve inlet pressure of 3500psig was located to identify its associated temperature. Equation (1) was used to determine the amount of heat removed from the incoming air if liquid is being produced

$$Q = mc_p(T_{hi} - T_{ci}) \quad (1)$$

Where m is the flowrate of the compressor, c_p is the isobaric heat capacity for air at compressor discharge (tube) pressure, T_{hi} is the temperature of the "warmer" air entering the RHX from the ice-water heat exchanger, and T_{ci} is the temperature of the cooled air entering the JT valve.

To determine the return air (shell side) outlet temperature, Equation (1) was rearranged and solved for T_h. as, shown in Equation (2)

$$T_{hs} = \frac{Q}{mc_p} + T_{cs} \tag{2}$$

where m is the flowrate of the return air, c_p is the isobaric heat capacity for air at atmospheric pressure, T_{cs} is the temperature of the expanded air returning from the dewar, and Q is the heat energy added to the returning air and must be equal to the heat removed from the incoming air. This revealed that to match the heat-load requirements on the tube side, the necessary shell-outlet temperature is 402K, which is not feasible. Limiting the shell-outlet temperature to be approximately equal to the tube-inlet temperature results in adjustment of the return air flowrate as the only option to match the required heat load. Flowrate adjustments were simulated in Microsoft Excel to determine their corresponding Heat Energy capacities due to system limitations, and are depicted in Figure 9.

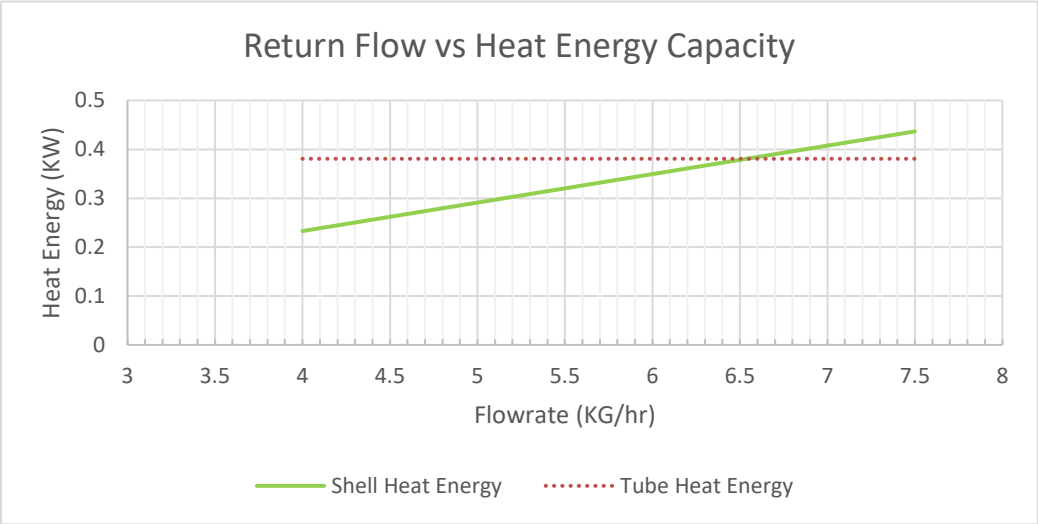

Figure 9. Shell Side Heat Load Capacity for Various Flowrates

The lower value of 4 kg/hr was the original system flowrate when dewar pressure was maintained at 10 psig. To achieve the required heat load-capacity, a flow rate greater than 6.5 kg/hr was required. This too would not be feasible with the current system, due to the current compressor's output capacity. The dewar pressure required to achieve this flowrate would also be well above the 20 psig set point of its included pressure relief valve.

Limiting the shell outlet temperature to be approximately equal to the tube inlet temperature allowed further performance analysis of the RHX based on its overall construction. Using Equation (3), a log mean temperature difference (LMTD) for the current system was calculated.

$$\Delta T_m = \frac{(T_{hi} - T_{hs}) - (T_{ci} - T_{cs})}{\ln \frac{(T_{hi} - T_{hs})}{(T_{ci} - T_{cs})}} \tag{3}$$

The LMTD is the thermal driving force for the heat exchanger and is the logarithmic average temperature for the hot and cold streams in the system (Primo 2012).

The heat transfer surface area of the RHX is calculated using Equation (4)

$$A_r = \pi d L \tag{4}$$

where d is the outer diameter of the stainless steel tubing and L is the overall length of the tubing inside the RHX. Applying the values calculated in equations (3) and (4) to equation (5), the overall heat transfer coefficient, U, required for the current system to meet the specified heat exchange needs was determined.

$$Q = U A_r \Delta T_m \tag{5}$$

Some of resultant values are significantly different from those reported by Nitro-Turbodyne and are displayed in Table 2.

Table 2. Thermodynamic Characteristics of Current System

	ΔTm (K)	Ar (m^2)	U ($W/m^2 \cdot K$)	Q (KW)
Reported	24.24	0.394	35	0.337
Calculated	24.88	0.608	15.32	0.232
Required	41.12	0.440	35	0.381

The calculated LMTDs were about equal based on the assumed shell outlet temperature. The overall heat transfer coefficient was calculated to be 15.32 $W/m^2 \cdot K$, about half the specified 35 $W/m^2 \cdot K$ (Nitro-Turbodyne 2016a). This alone solidified that the current setup does not have an adequate thermal driving force for the required heat exchange. The surface area required for the specified heat transfer coefficient is 0.44 m^2, where the current system provides 0.61 m^2 of surface area. In theory, the size of the RHX should be more than sufficient, but the previously identified departure from specification with the PTFE tubing diameter is hindering performance. This deviation restricted return airflow by only allowing a maximum of a quarter inch of flow area vice the specified half inch as designed. The smaller diameter restricted flow and prevented the laminar flow from fully developing. This in turn allowed a boundary layer to form on the tube walls and prevented thorough heat transfer across the stainless steel tubing wall. This had a parasitic effect on the overall efficiency of the RHX. This restriction increased the work required by the compressor due to the increased dewar pressures required to maintain adequate flow, again limiting the RHX efficiency.

To make current system match the provided specifications, it would require complete reconstruction of the RHX. This would eliminate the flow restriction on the shell side of the RHX. The compressor work would be reduced and allow more flexibility in return airflow adjustment. Correction of this fabrication misstep would increase the RHX heat transfer capacity from the previously calculated value of 0.232 KW to 0.529KW. This stepped improvement would theoretically allow JT inlet temperature to reach values around 139K if the overall heat transfer coefficient matched the specified 35 W/m^2K. Figure 10 is a plot of theoretical RHX performance if it operated at the specified overall heat transfer

coefficient up through the typical range of 60–180 W/m^{2}K for air-cooled heat exchangers (Primo 2012).

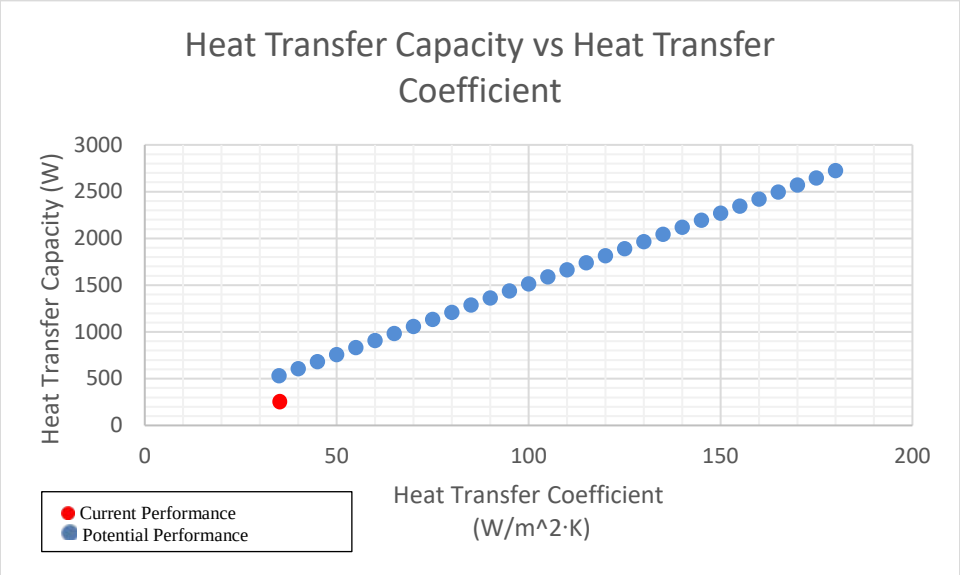

Figure 10. Specified Design RHX Heat Transfer Capacity with Typical Air-Cooled Heat Transfer Coefficients

At the lower end of the typical values for the heat transfer coefficient, the specified design would provide almost three times the required cooling capacity. This would ultimately result in shorter cool down times to liquefaction temperatures and more flexibility with return airflow rates. The greater performance would also compensate for small amounts of heat injection from ambient temperatures into the system through the installed insulation.

IV. NEW HEAT EXCHANGER PROPOSED DESIGNS

A. SPIRAL TUBE DESIGN

The proposed spiral tube design is an expansion on the current RHX design. It relies on a heat exchanger premanufactured by Sentry Equipment pictured in Figure 11.

Figure 11. Sentry Spiral Tube Heat Exchanger. Source: Sentry (2015).

The configurability of this heat exchanger's design is what made it a viable option. It provides the ability to specify material types, flow configurations, manufacturing tolerances to optimize it for this application without compromising overall efficiency. The most appealing attribute of this heat exchanger is its compact design at only six cubic feet. This will allow a seamless integration into future mobile applications.

The use of a premanufactured heat exchanger would eliminate some of the issues that were inherent to the handmade exchanger previously used. This heat exchanger is built to meet the American Society of Mechanical Engineers (ASME) standards and stamped with their approval. The channels and air gaps in the coiled tube bundle assembly create the shell side of the heat exchanger and eliminate the restrictive shell side of the previous design. The welded joint manufacturing process used in construction provides increased durability and strength. "The spiral shape of the flow for the tube side and shell side fluids creates centrifugal force and secondary circulating flow that enhances the heat transfer on both sides in true counter flow arrangement." (Sentry 2015, 1) The compact design and use

of a common manifold for the tube assembly eliminates the need for baffles and tubesheets found in conventional shell and tube heat exchangers. The coiled tube design allows for a footprint a fraction of the size of conventional shell and tube heat exchangers with comparable performance.

Figure 12 is a cross-sectional view of the spiral tube heat exchanger and identifies some of the specified design materials and dimensions to be used in construction.

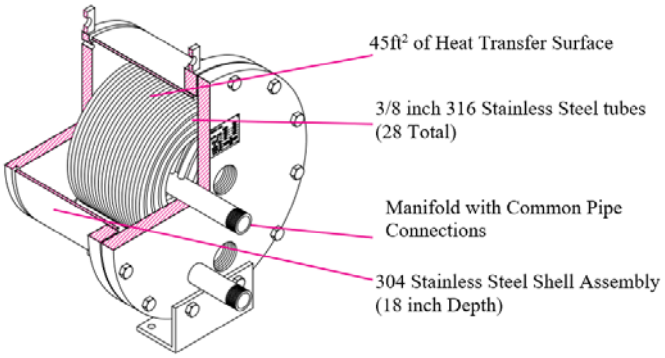

Figure 12. Cross-Section of a Spiral Tube Heat Exchanger. Adapted from Sentry Equipment (2015).

A heat transfer surface area of 45-ft^2 was chosen to ensure there was plenty of design margin if future iterations of the LAES system were to employ a higher capacity compressor. The overall size selection of the heat exchanger also would allow the potential of the current compressor to be maximized without a significant increase in overall system volume. To provide a significant improvement in thermal conductivity over the 304 stainless steel used in the current system, 316 stainless steel was chosen as the tube material. This advantage will assist in meeting and possibly exceeding the previous RHX overall heat transfer coefficient. It also provides improved corrosion resistance needed for future field deployed systems. Utilizing 3/8 inch tubing instead of 1/4 inch tubing for the tube bundle requires 14 less tubes, which equates to about 230 less linear feet of tubing. This material reduction aids in maintaining the heat exchanger as compact as possible. The use of common pipe connections for the manifolds would allow for simple integration and quick reconfiguration as needed. The stainless steel shell provides a rigid housing to protect

the heat exchanger as well as an ideal mounting surface to adhere insulation. A bolted vice welded housing was chosen to allow easy access to the tube assembly in the event it must be inspected or repaired.

Another proposed change for this configuration would be to install a smaller dewar. The previous 25-liter dewar will be replaced with a six liter dewar instead. This will provide a decrease in overall system volume to roughly half of the original design and more than compensate for the eight-liter increase in volume from the addition of the larger heat exchanger. This too will reduce the cool down times required to reach cryogenic temperatures.

The worst-case scenario would assume the overall heat transfer coefficient just matches the previously specified value of 35 $W/m^2 \cdot K$. At that value, this setup would still potentially provide about 3.66 kilowatts of heat transfer capacity. This is roughly seven times the original design and ten times the required capacity. Figure 13 is a performance comparison of the original design potential and the theoretical performance of the spiral tube exchanger across the typical range of heat transfer coefficients for air-cooled applications.

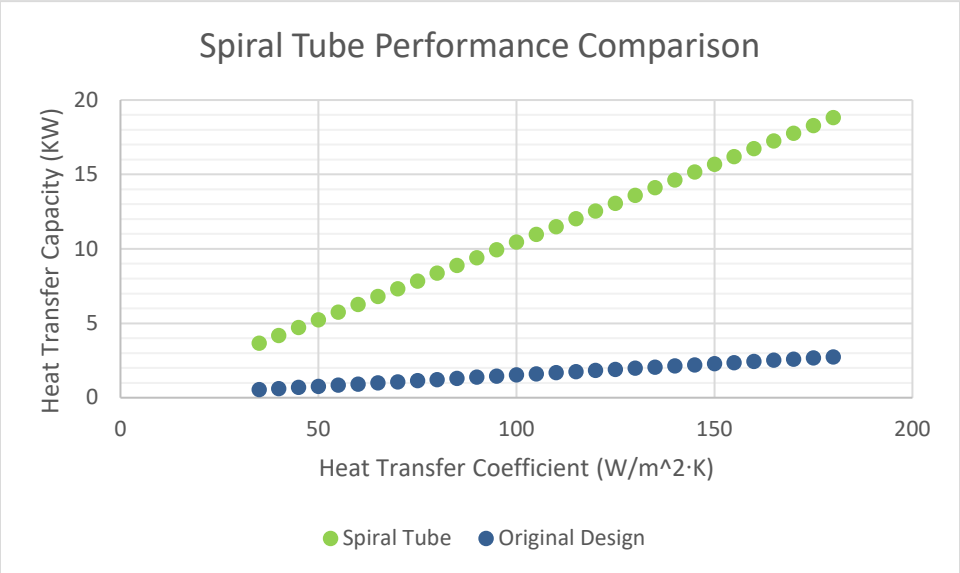

Figure 13. Performance Comparison of Original Design and Spiral Tube Exchanger

The worst-case performance for the spiral tube would still be about one kilowatt better than the best possible performance of the current design. The volume reduction and increased heat transfer capacity should allow for cool down times roughly one third to one-half of the original times.

One major drawback to this design is it would come with a premium cost. A one off cost of $30K could be enough to direct production elsewhere. Price reduction potential exists if the contract was extended for mass production. Another shortfall to this design is the sheer weight of heat exchanger. With about 460 linear feet of stainless steel tubing plus a stainless steel housing, the entire assembly would weigh approximately 800 pounds. This would require rigging to position the heat exchanger and potentially require trailering instead of mounting it to a utility cart. This would not remove the option of mobility, but it would limit some of the application potential.

B. FINNED TUBE DESIGN

The use of finned tubes in heat exchangers is more common in air-cooled applications or working fluids with relatively low heat transfer coefficients. Plain, or smooth, tubing in general is relatively inefficient at heat transfer. The addition of fins in a heat exchanger can increase the heat transfer surface area of the system up to 15 times without an increase in volume. This design would still be a double tube counter-current heat exchanger. A slightly larger shell would be required to accommodate the addition of fins, but this would have minimal effect on the actual flow area for the secondary side of the heat exchanger. Two options considered to develop this design were, complete in-house fabrication or the purchase prefabricated tube sections.

The self-fabrication option would produce a finned heat exchanger much like the one used for the ice-water heat exchanger. This would require hand forming a new coil with the correct pitch and diameter, cutting out each individual fin, drilling holes in each fin, and then attaching them to the new coil by either soldering or tension mounting with thermal paste. Tension mounting would require drilling holes in the fins slightly smaller than the outer tube diameter and then forcing them into position along the coil. With the tension method, there is risk of damaging the coil with installation of each fin requiring

complete rework at any time during the process. There is the potential for non-uniform fin size if not done through a machining process. Increased thermal resistance at the intersection of the tube wall and fin assembly due to the available attachment methods is possible as well. Any gaps between the fins and tube wall would significantly reduce heat transfer in those areas. In addition, the heat from the soldering process could result in weak points in the tubing, which could result in catastrophic failure with the high pressure on tube side of the heat exchanger. All of these issues could potentially cancel out the performance benefit of adding fins to the RHX.

The prefabricated tube sections appears to be the better option. Several types of finned tubes were explored to identify the ideal style for this application to include (Serth 2007, 632):

- Integrally finned
- Bimetallic
- Tension-wound fin
- Embedded fin
- Brazed fin

The integrally finned, or k-type fin, tubes are produced using an extrusion process. Since the fins are physically formed out of the tube walls, perfect thermal contact with any operational conditions is ensured. The material used for this process is usually copper or aluminum alloys due to having to be soft and easily workable. Although these materials have excellent heat transfer characteristics, neither of them can withstand the system's operating pressure of 3500 psig.

The bimetallic tubes are a two-part construction consisting of an inner tube and outer tube. The inner tube can be any typical tube material, but the outer tube is usually made of aluminum alloy. Due to imperfect contact between the inner and outer tube thermal resistance at this interface can account for up to 25% of the total thermal resistance of the

heat exchanger (Serth 2007). This inefficiency is not tolerable if the goal is to maximize the RHX performance.

Tension wound finned tubes are very common due to their low production cost. They are produced by wrapping fin material around the tube under tension and then forming it into an ‘I’ or ‘L’ shape as shown in Figure 14.

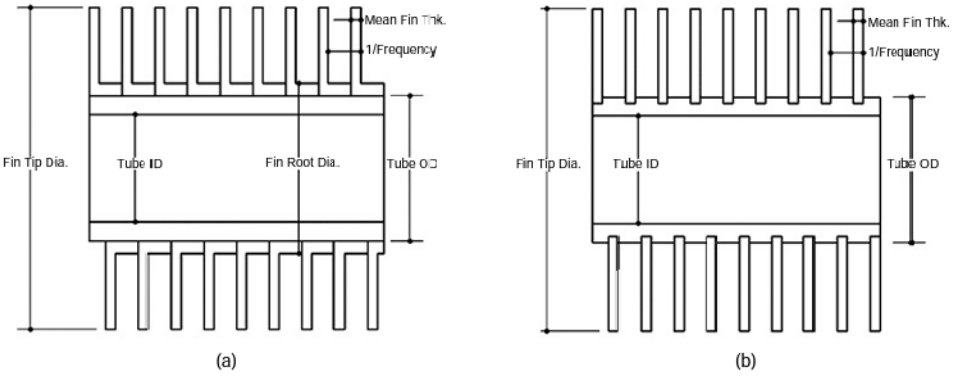

Figure 14. Tension Wound and Embedded Fin Tubes. (a) L-fin (b) I-fin similar to G-fin (pictured) but not embedded in tube wall. Adapted from Serth (2007).

The L-fin design provides greater contact area and is more resistant to corrosion on the tube wall than the I-fin. The fins are held in place and tension maintained by collars placed at either end of the tube. Because of this mounting technique, the fins are subject to loosening if exposed to cycling temperatures. Since moisture can penetrate between the fins and tube wall, they are also the most susceptible to corrosion.

Embedded fins are more common in cyclic application and are more robust than tension wound assemblies. They are formed by machining a groove in the tube wall, winding fin material into the groove, and then backfilling the groove with tube material (Serth 2007). To account for the groove made in the machining process, thicker tube walls are required. The groove also allows for the possibility of corrosion at base of the fins. Thicker tube walls and possible fin-root corrosion results in greater thermal resistance thus reducing the heat transfer capabilities in the heat exchanger.

Brazed-fin tubing eliminates most of the shortfalls of the other styles of finned tubes. It is constructed by first winding the fin material around the tube under tension just as it was for the tension-mounted style. The assembly is then placed in a controlled atmosphere brazing furnace to create a metallurgical bond between the tube and the fin metal. This process allows for the integration of dissimilar metals that normally cannot be combined through a welding process. The non-porous and uniform contact minimizes thermal resistance at the joints. The stress-free adhesion also allows for the use of thinner tube material than that used for welded joints. This robust assembly allows operation under severe conditions with temperatures as high as 1500˚F for stainless steel finned tubes. Figure 15 is a cross-sectional view of the brazed-fin tubing chosen for this design. The corrosion resistance, robust nature, and minimal thermal resistance make this fin type ideal for this application.

Figure 15. Brazed-Fin Tubing Cross-Sectional View. Source: Fin Tube Products (2016).

The tubing selected was a quarter-inch stainless steel tubing with six stainless steel fins per inch. The fins would be 0.015-inches thick and have a height of 3/16 of an inch. Two 20-foot sections of this tubing would provide just over 24-ft^2 of heat transfer surface area for this design. That is roughly four times the original design. The overall diameter of the finned tubes would require the shell-tubing diameter to increase to a 1.5-inch outside diameter tubing to maintain the half-inch flow area of the original design. The brazed-fin design would allow for coiling the tube with a mandrel pipe bender. At 40-linear feet, this

design would fit in a cylindrical housing a little larger than nine cubic feet and allow for mounting on a utility cart for ease of portability if coiled.

This design would utilize the smaller six-liter dewar as well. This would reduce the overall system volume to less than a quarter of the original design's volume. The heat exchanger volume would be about 40% of the original design, even with the larger diameter shell tubing. This volume reduction in addition to the increased surface area will decrease the time required to reach the required liquefaction temperature.

The overall heat transfer coefficient of this design should at least match that of the original design. At a value of 35 W/m^2K, this design should provide about 1.96 kilowatts of heat transfer capacity. That is over five times the required capacity and three and a half times the original design. Figure 16 is a plot is of the potential finned tube design theoretical performance compared to the original design potential.

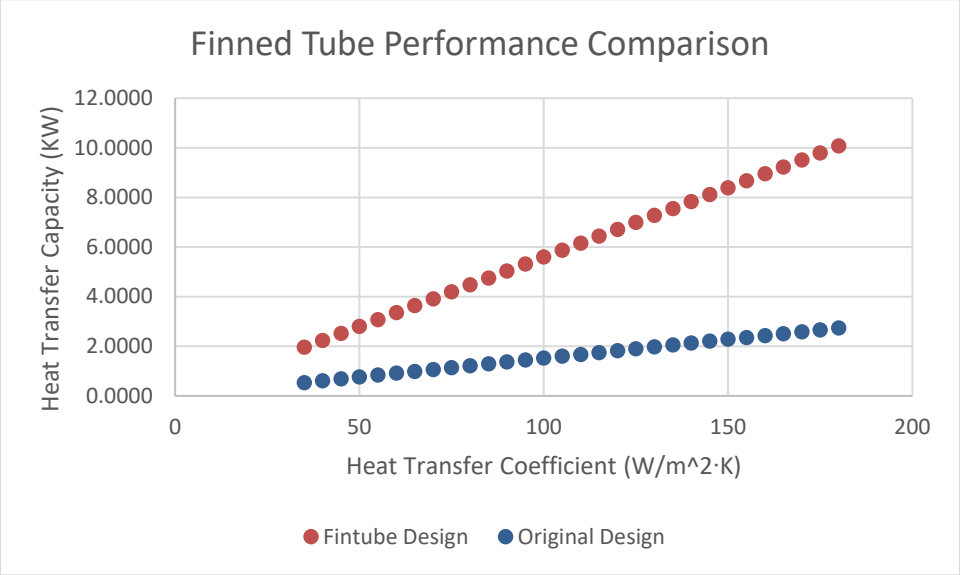

Figure 16. Finned Tube Potential Performance

The finned tube design performance at the original specified heat transfer coefficient would be equivalent to improving the original design to have a heat transfer coefficient of about 135 $W/m^{2\cdot}K$. The reduced volume should facilitate reaching liquefaction temperatures in about a quarter the amount of time required for the original design.

The major drawback to this design would be the need for some self-fabrication. The finned tubes ship in twenty-foot straight sections that require the addition of connection fittings as well as hand bending. If bend radius restrictions are not observed, the tubing could be damaged beyond repair and require replacement of an entire section. With a cost of one-thousand dollars per section, a simple mistake could quickly get expensive. The possibility of introducing leaks at the connection fittings is highly probable with incorrect installation or improper tightening. A minor leak could prevent the heat exchanger from meeting the current system's performance if not detected. This design risks repeating several of the issues that hindered the performance of the original design. If care is taken throughout the manufacturing process, the performance and size improvements would far outweigh the risks.

THIS PAGE INTENTIONALLY LEFT BLANK

V. CONCLUSION AND FUTURE WORK

This thesis provides the motivation and background for the construction and operation of a small-scale LAES prototype system. A prototyped system is essential in the MBSE process to verify individual components and their related subsystems to fully validate the system's functional decomposition.

This work started with the component identification during reconstruction and basic system operation of the system currently in NPS's possession. Initial reconstruction and operation was done in accordance with Nitro-Turbodyne's provided guidance. Theoretical analysis previously conducted by Howe (2017) provided the knowledge base necessary to test the limitations of the current system. It also assisted in identifying that a departure from specification in RHX during original construction is what resulted in the system's previous failure. Thermodynamic analysis was conducted to determine how large of an impact this change did have on overall system performance. Operational analysis was performed to explore the effects various system controls have on overall system performance. The operational analysis showed that increased flow rates resulted in better system performance, but the required flow for the current system configuration was beyond the capacity of the installed compressor. This analysis was essential in providing the operational data that was not available for previous research.

Chapter IV proposed two potential redesigns for the RHX. The first was a premanufactured spiral tube heat exchanger. This method would eliminate all the fabrication shortfalls of the original system and provide ten times the necessary cooling capacity. One of the major drawbacks is the excessive weight that would come with a heat exchanger of this size. Although it only occupies six cubic feet, the sheer weight could potentially limit its range of applications. It also would come at a cost of just over eight dollars per watt of thermal capacity. The second potential design change was a finned tubed design that utilized a braze-fin construction. This design would provide four times the surface area at less than half the volume of the original heat exchanger. The major drawback to this approach would be the need for some self-fabrication. This would lend to the introduction of some of the downfalls of the current system. This would still be a highly

viable option since it would be less than half the cost per watt of the spiral tube design. The ultimate decision would reside on how much risk the stakeholder is willing to accept for improved performance.

LAES systems directly support DoD's goal of energy resilience through reduced demand on fossil fuels. It also provides the energy generation characteristics necessary to improve the mobility of troops downrange. The work in this thesis reconstructed a LAES system in NPS's possession to provide operational data necessary to correct and improve the design of the small-scale LAES. Once operational, the data from this prototype would provide a standard for future designs in the MBSE process since there is not a commercially operated system of this scale.

Future work includes producing a functioning prototype through the correction of the original design to meet design specification, or implementation of one of the proposed design changes. Follow on students will continue modeling and simulation as necessary to fully explore the trade-space of a sustainable building scale system for stateside DoD facilities.

LIST OF REFERENCES

AireTex. 2006. “AireTex 45 High Pressure Breathing Air Compressor. Accessed April 01, 2019. http://www.airetex.com/paintball.php.

Ameel, Bernd, Christophe T’Joen, Kathleen De Kerpel, Peter De Jaeger, HenkHuisseune, Marnix Van Belleghem, and Michel De Paepe. 2013.”Thermodynamic Analysis of Energy Storage with a Liquid Air Rankine Cycle.” *Applied Thermal Engineering* 52: 130–140.

ASAIE, Department of the Army. 2015. *Energy Security and Sustainability Strategy.*RefID: 2–204FF1C. March 03. https://www.army.mil/e2/c/downloads/394128.pdf.

Barron, Randall F. 1985. *Cryogenic Systems.* 2nd. New York: Oxford University Press.

Blanchard, Benjamin S., and Wolter J. Fabrycky. 2010. *Systems Engineering and Analysis.* Upper Saddle River, NJ.: Pearson.

Castillo, L., and C.A. Dorao. 2013. “On the Conceptual Design of Pre-Cooling Stage of LNG Plants Using Propane or Ethan/Propane Mixture.” *Energy Conversion and Management* 140–146.

Douquet, Greg. 2017. “Unleash Us From the Tether of Fuel.” Atlantic Council. January 11, 2017. Accessed May 01, 2019. https://www.atlanticcouncil.org/blogs/defense-industrialist/unleash-us-from-the-tether-of-fuel.

Fin Tube Products. 2016. “Finbraze Finned Tubing.” Accessed April 28, 2019. http://www.fintube.com/finbraze-tubing.html.

Hands, B. A., ed. 1986. *Cryogenic Engineering.* London: Academic Press Inc.

Hicks, Sierra. 2017. “Fact Sheet: Powering the Department of Defense.” American Security Project. September 18, 2017. https://www.americansecurityproject.org/fact-sheet-powering-the-department-of-defense/.

Howe, Todd A. 2018. “Thermodynamic System Analysis of a Liquid Air Energy Storage System.” Master’s thesis, Naval Postgraduate School. https://calhoun.nps.edu/handle/10945/59687.

Kim, Young-Min, Jang-Hee Lee, Seok-Joon Kim, and Daniel Favrat. 2012. “Potential and Evolution of Compressed Air Energy Storage: Energy and Exergy Analyses.” *Entropy* 14, no. 8: 1501−1521. https//: doi:10.3390/e14081501

Lemmon, E.W., M.O. McLinden, and D.G. Friend. 2008. *NIST Chemistry WebBook, NIST Standard Reference Database Number 69.* Eds. P.J. Linstrom and W.G. Mallard, National Institute of Standards and Technology. http://webbook.nist.gov/chemistry/fluid/.

Lemmon, Eric W., Richard T Jacobsen, Steven G. Penoncello, and Daniel G. Friend. 2000. "Thermodynamic Properties of Air and Mixtures of Nitrogen, Argon, and Oxygen from 60 to 2000 K at Pressures to 2000 MPa." *Journal of Physical and Chemical Reference Data* (American Institute of Physics) 29, no. 3 (2000): 331–85. https:// doi.org/10.1063/1.1285884

Marine Corps Expeditionary Energy Office. 2011. Marine Corps Expeditionary Energy Strategy and Implementation Plan. Washington, DC: Marine Corps Expeditionary Energy Office Headquarters.

McLarnon, Frank R., and Elton J. Cairns. 1989. "Energy Storage." *Annual Review Energy* 14: 241–271.

Moran, Michael J., and Howard N. Shapiro. 2004. *Fundamentals of Engineering Thermodynamics.* 5th. Hoboken, NJ: John Wiley & Sons

Navy Office of Information. January 21, 2010. "USDA, Navy Sign Agreement to Encourage the Development, Use of Renewable Energy." Accessed April 15, 2019. https://www.navy.mil/submit/display.asp?story_id=50710.

Nitro-Turbodyne, Inc. 2016a. "Process Flow Diagram (P&ID) LAESS." Revision 2. January 22, 2016.

Nitro-Turbodyne, Inc. 2016b. "Operations Manual Liquid Air Energy Storage System (LAESS)." Under Noble Supply Purchase Order P659307 for Naval Facilities Command Engineering and Expeditionary Warfare Center, August 12, 2016.

Office of the Chief of Naval Operations. 2012. OPNAV Instruction 4100.5E. Department of the Navy. https://navysustainability.dodlive.mil/files/2012/07/OPNAVINST-4100.5E.pdf.

Office of the Assistant Secretary for Defense (OASD) for Sustainment. n.d. "Operational Energy." Accessed April 10, 2019. https://www.acq.osd.mil/eie/OE/OE_index.html.

Office of the Assistant Secretary of Defense for Energy, Installations and Environment. (2017). *Annual Energy Management and Resilience (AEMR) Report*. 7. https://www.acq.osd.mil/eie/Downloads/IE/FY%202017%20AEMR.pdf

Pollman, A.G. 2013. "Energy Optimization: A Combat Multiplier." *Marine Corps Gazette* 97(11): 69–73.

Primo, Jurandir. 2012. Class notes for M371: Shell and Tube Heat Exchangers-Basic Calculations. PDHOnline, Fairfax, VA. https://www.pdhonline.com/courses/m371/m371content.pdf.

Sentry Equipment. "Sentry Spiral Tube Heat Exchanger." Accessed May 13, 2019. https://sentry-equip.com/sentry-spiral-tube-heat-exchanger.html.

Serth, Robert W. 2007. *Process Heat Transfer Principles and Applications*. Amsterdam: Elsevier. Electronic.

United States Army. 2015. Energy Security & Sustainability Strategy. Department of the Army. https://www.army.mil/e2/c/downloads/394128.pdf

United States Navy. 2018. Navy Shore Energy Program. Accessed January 2018. https://www.cnic.navy.mil/om/base_support/facility_system_investment/Navy_Shore_Energy_Program.html.

Wang, S.X., X.D. Xue, X.L. Zhang, J. Guo, Y. Zhou, and J.J Wang. 2015. "The Application of Cryogens in Liquid Fluid Energy Storage Systems." *Physics Procedia* 67: 728−732. https//:doi.org/10.1016/j.phpro.2015.06.123.

Willis, Ryan. Forthcoming. "Modeling of a Building-Scale Liquid Air Energy Storage System with Aspen HYSYS." Master's thesis, Naval Postgraduate School. https://calhoun.nps.edu/handle/10945/17

THIS PAGE INTENTIONALLY LEFT BLANK

INITIAL DISTRIBUTION LIST

1. Defense Technical Information Center
   Ft. Belvoir, Virginia

2. Dudley Knox Library
   Naval Postgraduate School
   Monterey, California